Desalination and Water Treatment
www.deswater.com

doi: 10.5004/dwt.2018.21950

108 (2018) 329–337
March

A fast adsorption of methylene blue by tobacco rob residues from aqueous solutions

Hefang Wang, Zetao Shi, Mengmeng Duan, Yansu Wang, Luming Wu, Cunyue Wang, Yongfang Yang*

School of Chemical Engineering and Technology, Hebei University of Technology, Tianjin 300130, China, email: wuyuyang123456@163.com (Y. Yang)

Received 16 August 2017; Accepted 24 January 2018

ABSTRACT

Tobacco rob residues (TRR) were used as an adsorbent for the adsorption of methylene blue (MB) from aqueous solutions. The structure and morphology of the TRR were characterized by Fourier-transform infrared spectroscopy, X-ray diffraction, Zeta potential and N_2 adsorption–desorption. The effect of contact time, pH, tobacco rob residues dosage, sodium chloride (NaCl) concentration and initial concentration of MB were investigated by a series of static adsorption experiment. Meanwhile, the adsorption isotherms were determined and fitted by Langmuir and Freundlich adsorption isotherm. The results confirmed that the adsorption isotherm data fitted well to Langmuir isotherm with monolayer adsorption capacity of 233.3 mg/g. The adsorption processes were studied by pseudo-first order, pseudo-second order and intra-particle diffusion kinetic models. And the adsorption kinetics was found to follow a pseudo-second order kinetic model. TRR also have the advantages of facile recovery and recycle. Thus, TRR is potential to be used as a good natural adsorbent.

Keywords: Adsorption; Tobacco rob residue; Methylene blue; Zeta potential

1. Introduction

Dyes are mainly used in textiles, rubber, paper, plastics, cosmetics and pharmaceutical industries. Today, the dye species used commercially are more than 10,000 [1]. The discharge of waste water containing dyes can not only reduce light phenomena, but also increase the toxicity and chemical oxygen demand (COD) of the effluent [2], which can result in great harm to aquatic organisms [3–5]. Therefore, the treatment of dye wastewater is imminent and has become a very important issue. Methylene blue (MB) [6] is an important cationic dye, which is widely used in coloring paper, temporary hair colorant, dyeing cottons, wools and coating for paper stock [7]. MB ingested or inhaled may cause many problems such as nausea, vomiting, diarrhea, dyspnea, tachycardia, cyanosis and methemoglobinemia [8].

The conventional methods for the treatment of MB waste water are coagulation and flocculation, oxidation or ozonation, membrane separation, biological treatment and adsorption [9–12]. Among them, the adsorption is an important method to treat the MB wastewater owing to its low cost and high removal efficiency. Therefore, an efficient and economical adsorbent could be important for the treatment of the MB waste water.

Activated carbon has been used in the adsorption of MB with large adsorption capacity and high adsorption efficiency [4,13,14]. However, the high cost and the air pollution (carbon monoxide and dust) in the activated carbon production restricts the application for adsorption of MB. Various agricultural and forestry wastes, such as seaweed [15], waste tea [16], peanut shell [1], rice husk [17], phoenix tree leaf powder [18], *Platanus orientalis* leaves [19], sawdust [20] and wheat straw [21] have been used for adsorption of MB from aqueous solutions and some of them have good adsorption property.

* Corresponding author.

Tobacco plants were cultivated widely in the world as a main material to make cigarette. Tobacco rod (TR) accounts for 60% of the tobacco weight. TR was burned or thrown as waste in the cigarette production and it was not only a waste of resources but also a source of pollution in the environment. Our previous work indicated that tobacco rob extract could be used as an efficient corrosion and scale inhibitor in seawater and circulating cooling water [22,23]. The application of untreated agricultural or forestry waste as adsorbents can also bring several problems such as low adsorption capacity, high COD and biological oxygen demand as well as total organic carbon due to release of soluble organic compounds contained in the plant wastes. In addition, the residue of extraction of TR is rich in cellulose and lignin and contains functional groups of hydroxyl and carboxyl. Herein, the tobacco rob residues (TRR) could be used as an adsorbent for removal of MB. The adsorption of MB onto TRR from aqueous solution is studied in this paper, which was obtained after extracting TR. The effects of the MB solution concentration, contact time, pH, adsorbent dosage and NaCl concentration were studied. The adsorption was analyzed using different isotherms and kinetic models. X-ray diffraction (XRD), scanning electron microscopy (SEM), Fourier-transform infrared (FT-IR) absorption spectra, Zeta potential and N_2 adsorption–desorption were used for the characterization of TRR.

2. Experimental setup

2.1. Materials

Tobacco rob was obtained from Lingshou County (38.31°N, 114.38°E), Hebei Province, China. All the reagents were of analytical purity. MB, sodium hydroxide (NaOH), hydrochloric acid (HCl), ethylenediaminetetraacetic acid (EDTA) and sodium chloride (NaCl) were purchased from Sinopharm Chemical Reagent Co., Ltd., China.

2.2. Preparation of TRR

The dried tobacco rob powder (8.0 g) was soaked in flask of three necked with distilled water (100 mL) and refluxed for 2 h at 100°C. After cooling to room temperature, the mixture was filtered and dried the filter residue at 105°C for 12 h. The particle size of the TRR powder is in the range of 0.15–0.3 mm for the adsorption of MB.

2.3. Components of TRR

The main components of TRR were analyzed by the method of Chen et al. [24]. Moisture content, volatile matter, ash content and fixed carbon of TRR were determined. The crucible with 1.0 g of TRR was dried at 105°C for 1 h in an oven. The loss of weight of TRR was reported as percentage moisture content. The remaining sample (covered with lid) was placed in a muffle furnace at 925°C for 7 min. The loss of weight was reported as volatile matter. The TRR residue (without lid) was heated at 700°C for 30 min. The loss of weight was reported as ash and the remaining sample was determined as fixed carbon likely containing a little of other ions, such as Ca^{2+} and Si^{2+}. Bulk density was calculated by weighing 100 cm^3 of sample. Above analysis was carried out thrice and the average values were shown as Table 1.

2.4. Characterization of the adsorbents

FT-IR absorption spectra were obtained on a Bio-Rad FTS 6000 system using diffuse reflectance sampling accessories. Powder XRD patterns were obtained using XRD, D/max-2500 with Cu Kα radiation, λ = 1.5406 Å). Brunauer–Emmett–Teller (BET) surface area analysis was performed using the nitrogen adsorption isotherms at 77 K using a Micromeritics Model ASAP 2020 instrument. All samples were degassed at 423 K under vacuum for 6 h. The average pore diameter and pore volume were calculated based on the Barrett–Joyner–Halenda method.

2.5. Preparation of MB solution

The 2,000 mg/L methylene blue solution was prepared as a stock solution. All experimental solutions were prepared by diluting the stock solution with distilled water to the required concentration. HCl (0.1 M) and NaOH (0.1 M) were used to adjust the acidity of the medium.

2.6. Adsorption experiments

Adsorption experiments were carried out in a series of 150 mL conical flask containing certain quality TRR and 50 mL MB solution in different concentrations. The mixture solution was stirred in the thermostat water bath. At preset time, the flask was taken out from the thermostat water bath. Residual dye concentration in the reaction mixture was analyzed using a UV-visible spectrophotometer at a maximum wavelength of 665 nm.

Calculation formulas of removal rate (r) and adsorption capacity (q_t) are as follows:

$$r = \frac{c_0 - c_t}{c_0} \times 100\% \quad (1)$$

Table 1
Main components and physical properties of TRR

Components analysis	Content (wt %)	Element analysis	Content (%)	Physical properties	Content
Moisture content	8.14	C	36.0	BET surface area	15.3 m^2/g
Volatile matter	81.3	H	5.90	Pore volume	0.00834 cm^3/g
Ash	0.250	N	1.32	Pore diameter	4.77 nm
Fixed carbon	10.3	Ca	3.65	Bulk density	228 g/L
Cellulose	31.6	Si	0.581		
Lignin	35.5				

$$q_t = \frac{(C_0 - C_t)V}{m} \quad (2)$$

where C_0 and C_t (mg/L) are the liquid-phase concentration of the MB at initial and at any time of t, respectively. V is the solution volume (L) and m is the mass of the adsorbent (g).

3. Results and discussion

3.1. XRD data

XRD patterns of TRR are shown in Fig. 1. The XRD pattern of TRR shows that a strong peak at 21.8° is attributed to the (002) plane of the cellulose crystalline plane [25,26]. The peak at 15.3° is connected to the (101) plane of cellulose, which is in agreement with the previous works [26]. The cellulose with the functional groups of hydroxyl and carboxyl can be the potential functional groups for the adsorption of MB.

3.2. SEM image

Fig. 2 shows the SEM of the TRR before (a) and after (b) MB adsorption. It can be seen clearly that the surface of the TRR is rough, which is possible for the adsorption of the MB. As shown in Fig. 2(b), it is clear that the surface of the TRR is covered by the MB.

3.3. Surface area and pore structure

The pore size distribution curve of TRR is shown in Fig. 3. The BET surface area of TRR is 15.3 m^2/g and the average pore size of TRR is 4.77 nm. The pore volume is 0.00834 cm^3/g. It indicates that the TRR has a mesoporous structure, which facilitates the adsorption of MB.

3.4. FT-IR spectra

The FT-IR spectra before and after adsorption of MB are shown in Fig. 4. The strong band at 3,425 cm^{-1} is associated to the stretching vibration of –OH, which can be from cellulose and lignin [27]. The characteristic bands at 2,925 and 2,926 cm^{-1} are assigned to the aliphatic C–H stretching vibration [28]. The band at 1,628 cm^{-1} is due to the C=O stretching vibration from carboxylic acid with intermolecular hydrogen bond [29]. The band at 1,426 cm^{-1} is attributed to the C–O stretch vibration in the carboxylic acid [30]. The band at 1,318 cm^{-1} is related to –OH in-plane vibration in the secondary alcohol. The band at 1,060 cm^{-1} may be –OH bending vibration or C–O–C stretching vibration in lignin structure [29]. The band at 619 cm^{-1} is due to C–OH out-plane bending vibrations.

After adsorption of MB, the peak of the C=O stretch vibration of carboxylic acid shifts from 1,628 to 1,605 cm^{-1} [29]. The peak at 1,426 cm^{-1} of C–O in the carboxylic acid shifts to

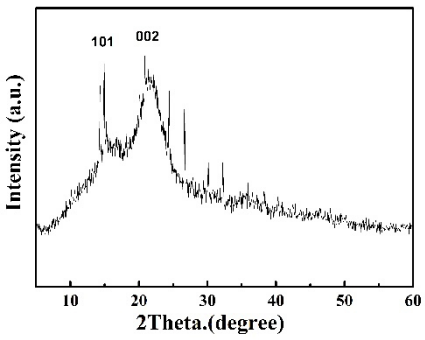

Fig. 1. XRD patterns of TRR.

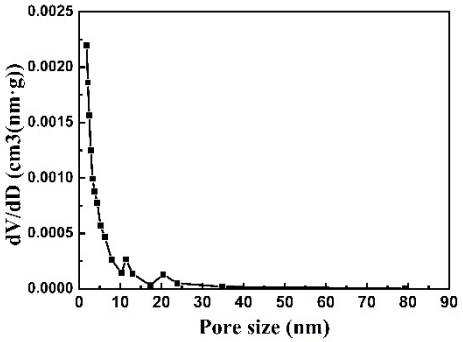

Fig. 3. Pore size distribution curve of TRR.

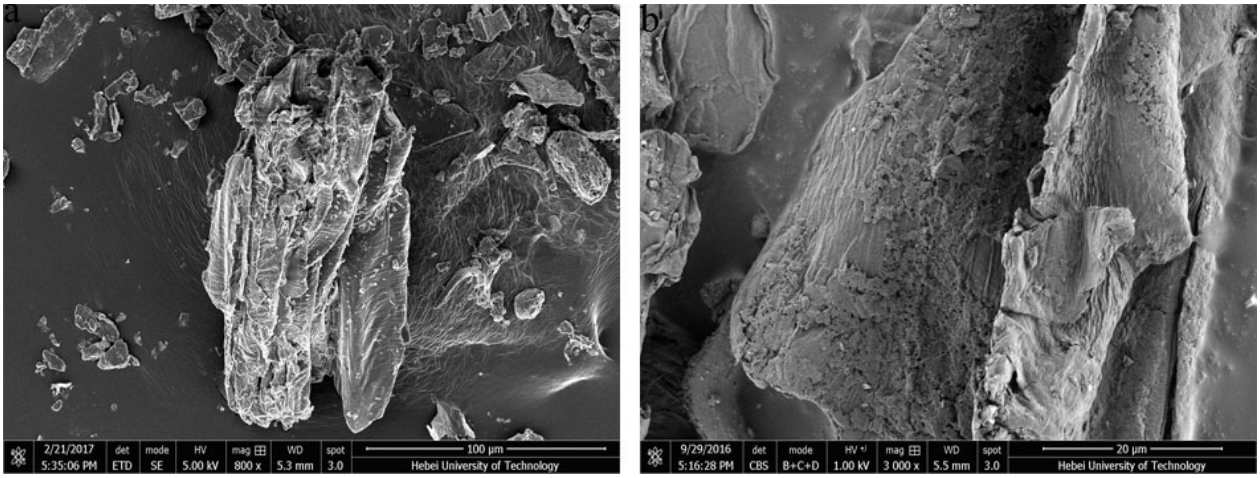

Fig. 2. SEM images of TRR before (a) and after (b) adsorption of MB.

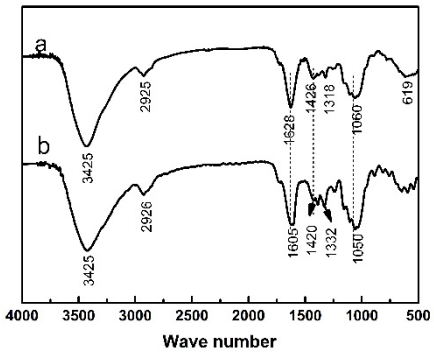

Fig. 4. FT-IR spectra of tobacco rob residues before (a) and after (b) MB adsorption.

1,420 cm^{-1}. The banding vibration of –OH shifts from 1,060 to 1,050 cm^{-1}. The results of FT-IR indicate that hydroxyl group and carboxyl group could be the main adsorption functional groups for the adsorption of MB onto TRR.

3.5. Adsorption test

3.5.1. Effect of the MB solution concentration and contact time on the MB adsorption onto TRR

The effects of initial MB concentration (50–250 mg/L) on adsorption of MB were investigated (shown in Fig. 5(a)). The experiments were conducted at 25°C with pH at 6.5 and TRR dosage of 5.0 g/L. The equilibrium adsorption capacity increases from 7.53 to 43.8 mg/g with the increase of initial MB concentration from 50 to 250 mg/L, which is due to that the initial concentration of MB in solution provides the necessary driving force to overcome the resistance to mass transfer of the MB between the aqueous phase and the solid phase [31]. An increase in the initial MB concentration also enhances the interaction between MB and TRR. Therefore, an increase of initial MB concentration leads to an increase of the adsorption capacity of TRR. In addition, the adsorption rate is very fast in the first 3 min. The adsorption equilibrium time is about 10 min in the investigated adsorption condition, which is attributed to that there are abundant adsorption sites on the adsorbent at the initial stage of adsorption. Such a fast adsorption rate could be referred to the absence of internal diffusion resistance [32]. To be sure that full equilibrium was attained, the experimental data were measured at 30 min.

3.5.2. Effect of the initial pH on adsorption of TRR

The initial pH is an important factor which affects the adsorption of MB onto TRR. The effect of pH on the removal of MB has been investigated at pH of 2.0–11.0 (shown in Fig. 5(b)). The experiments were conducted at 25°C with initial concentration of 50 mg/L and TRR dosage of 5 g/L. The removal efficiency of MB onto TRR increased from 40.2% to 78.6% after the pH increased from 2 to 11. The removal efficiency increased rapidly from 40.2% to 72.3% with the pH increased from 2 to 5.5. The removal efficiency increased slowly from 72.3% to 78.6% with the further increase of pH from 5.5 to 11.0. Moreover, the results of Zeta potential show that the TRR surface charge was zero at pH of 2.0. And the

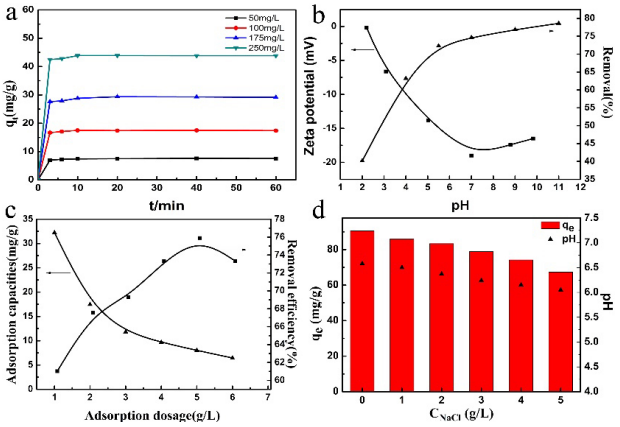

Fig. 5. Effects of contact time and initial concentration (a), pH (b), TRR dosage (c) and ionic strength (d) on the adsorption of MB onto TRR.

surface charge of TRR is negative when the pH greater than 2.0, which indicates that the high pH is benefit for the adsorption of MB (cationic dye). In addition, the concentrations of H^+ are high under low pH and abundant H^+ and the MB cation might compete for the adsorption sites (Eqs. (3) and (4)). Therefore, high pH is in favor of the MB on TRR through electrostatic forces of attraction [16]. The following studies were conducted at a fixed pH of 7.0.

$$TRR^- + MB^+ \xrightarrow{pH=7} TRR - MB \quad (3)$$

$$TRR^- + MB^+ + H^+ \xrightarrow{pH=2} TRR - MB + TRR - H \quad (4)$$

3.5.3. Effect of the adsorbent dosage on the adsorption of TRR

Effect of the TRR dosage was investigated at 25°C, initial MB concentration of 50 mg/L and at pH 7 (shown in Fig. 5(c)). The result shows that MB removal efficiency increased slowly from 61.0% to 75.9% with the TRR dosage increase from 1.0 to 5.0 g/L. This can be attributed to that the adsorbent surface area and adsorption sites increased resulting from the increase of adsorbent dosage (1.0–5.0 g/L). However, the removal decreased to 73.3% with the TRR dosage increase to 6.0 g/L, which is due to the reduction of adsorption sites for the agglomeration of the TRR. It can be seen from Fig. 5(c) that the adsorption capacity decreases with the increase of adsorbent dosage. It is due to the competition between adsorbent and the split in the concentration gradient [29,33] and the decrease of MB molecular on unit adsorption sites.

3.5.4. Effect of NaCl concentrations on the adsorption of TRR

The effect of the NaCl concentrations on the adsorption of MB onto TRR was studied at the concentrations of NaCl (1.0, 2.0, 3.0, 4.0 and 5.0 g/L) contained in the 500 mg/L MB solution (shown in Fig. 5(d)). As seen in Fig. 5(d), with the concentration of NaCl increases from 0 to 5.0 g/L, the adsorption capacities were decreased from 90.5 to 67.3 mg/g, which can be due to the competitive effect for the adsorption sites

between MB ions and Na^+ [27] on the one hand, and on the other hand, the electrostatic interaction of adsorbent surface active sites and MB may be screened by the Na^+ released from NaCl [29]. The pH decreased from 6.58 to 6.05 with the increase of NaCl concentration, which may due to the H^+ and lower hydrolyze constants cation (such as Ca^{2+}) released from the surface of adsorbent to aqueous solution [24].

3.5.5. Adsorption kinetics

The kinetic parameters are helpful for predicting the adsorption mechanism and the adsorption rate of the adsorbent. To investigate the adsorption kinetics of MB on TRR, the adsorption kinetics data of MB adsorption onto TRR were used for the fitting of the pseudo-first order and pseudo-second order equation which are expressed as follows:

Pseudo-first order model:

$$\ln(q_e - q_t) = \ln q_e - k_1 t \quad (5)$$

where q_e and q_t are the amounts of MB adsorbed at equilibrium and at any time of t (mg/g) and k_1 is the equilibrium rate constant of pseudo-first order equation (min^{-1}).

Pseudo-second order model:

$$t/q_t = 1/(k_2 q_e^2) + t/q_e \quad (6)$$

where k_2 is the rate constant of adsorption (g/(mg·min)) of pseudo-second order adsorption process.

The best-fit model was selected by the Chi-square (χ^2) test which is expressed as following:

$$\chi^2 = \frac{\sum (q_{e,\exp} - q_{e,\mathrm{cal}})^2}{q_{e,\mathrm{cal}}} \quad (7)$$

where $q_{e,\exp}$ (mg/g) and $q_{e,\mathrm{cal}}$ (mg/g) are the amount of dye adsorbed at equilibrium from experiment and mathematical model, respectively.

The fitting plots for the adsorption of MB onto TRR are shown in Fig. 6 and Table 2. The correlation coefficients for the second-order kinetics model (R^2 = 0.9999) are higher and the χ^2 (6.5×10^{-6} – 1.9×10^{-4}) are smaller than the pseudo-first order model (R^2 = 0.3840–0.8679, χ^2 = 146.9–1,261.1), which indicates better model predictability with less error for pseudo-second order kinetic model. In addition, the calculated equilibrium adsorption capacity is in well agreement with experimental data. This suggests that the rate-determining step of the adsorption mechanism is attributed to chemical sorption, and that mass transfer in the solution is not involved. The values of the rate constant, k_2, decrease with the increase of initial MB concentration. The reason for this behavior is that there is less competition for sorption sites at lower concentrations.

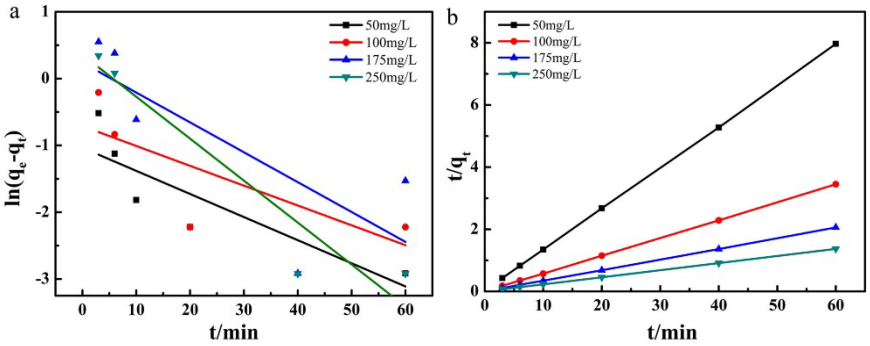

Fig. 6. Applicability of pseudo-first order (a) and pseudo-second order (b) kinetic models in the MB adsorption onto TRR.

Table 2
Parameters of the pseudo-first order and pseudo-second order kinetic models

Kinetic models	Model parameters	Initial concentration C_0 (mg/L)			
		50	100	175	250
Pseudo-first order	k_1 (min^{-1})	0.0346	0.0297	0.0447	0.0628
	$q_{e,\mathrm{cal}}$ (mg/g)	0.3556	0.4909	1.2694	1.4289
	$q_{e,\exp}$ (mg/g)	7.584	17.497	29.361	43.878
	$R2$	0.6665	0.3840	0.4779	0.8679
	χ^2	146.9	589.1	621.7	1,261.1
Pseudo-second order	k_2 (g/(g min))	0.9417	0.5929	0.3164	0.2331
	$q_{e,\mathrm{cal}}$ (mg/g)	7.577	17.44	29.29	43.90
	$q_{e,\exp}$ (mg/g)	7.584	17.497	29.361	43.878
	R^2	0.9999	0.9999	0.9999	0.9999
	χ^2	$6.5 \times {}^{10}$–6	$1.9 \times {}^{10}$–4	1.7×10^{-4}	1.1×10^{-5}

The adsorbate species could be conveyed from the solution into the adsorbent through an intra-particle diffusion process. In some adsorption processes, the intra-particle diffusion process is the rate-determining step. The intra-particle diffusion process was studied by intra-particle diffusion model which is expressed as following:

$$q_t = kt^{1/2} + C \tag{8}$$

where the k is the intra-particle diffusion rate constant (mol/(g·min$^{1/2}$)), C is the intercept.

The linear plots of q_t vs. $t^{1/2}$ are shown in Fig. 7. The values of k, C and the correlation coefficients (R^2) are summarized in Table 3.

If the correlation coefficient is high and the line passes through the origin, it can be said that the intra-particle diffusion is the sole rate-determining step [5]. However, the correlation coefficients in different concentrations are all less than 0.827, the intercepts C are not zero but large values (6.93–42.0 mg/g), which increases with the increase of initial MB concentrations. The results indicate that the boundary layer diffusion may be the rate-determining step in the MB adsorption process for TRR and it is more dominant when initial MB concentration is high [34].

3.5.6. Adsorption model of MB

The adsorption isotherms play an important role in the adsorption systems [35]. The Langmuir adsorption isotherm and Freundlich isotherm are wide applied in describing how adsorbates interact with adsorbents.

The Langmuir isotherm and Freundlich isotherm are expressed as follows, respectively.

$$q_e = \frac{q_m b C_e}{1 + bC_e} \tag{9}$$

$$q_e = K_F C_e^{1/n} \tag{10}$$

where the q_m is the maximum monolayer adsorption capacity and b is the constant of the Langmuir isotherm, which is related to the free energy of adsorption. The K_F and n are Freundlich adsorption isotherm constants. The K_F can roughly indicate the extent of the adsorption, and n is a constant which can indicate the degree of nonlinearity between solution concentration and adsorption.

The fitting of the isotherms were shown in Fig. 8. The parameters are presented in Table 4.

The results suggest that the Langmuir isotherm has lower χ^2 (0.918) and higher R^2 (0.959) than Freundlich isotherm (χ^2 = 9.812, R^2 = 0.902). It indicates that the Langmuir isotherm is a better fit model to describe adsorption equilibrium, and the adsorption of MB onto TRR is monolayer adsorption and the surface of TRR is homogenous [2]. The maximum adsorption capacity for methylene blue onto TRR is 233.3 mg/g. The n values of Freundlich isotherm show the favorability of sorption. That the values of the n can indicate the adsorption is good ($2 < n < 10$), moderately difficult ($1 < n < 2$), and poor sorption ($n < 1$), respectively. The value of the n in the adsorption of MB onto TRR is 2.60, which indicates that the adsorption of MB onto TRR is favorable.

In order to further express whether the adsorption system is favorable or unfavorable by Langmuir isotherm. The

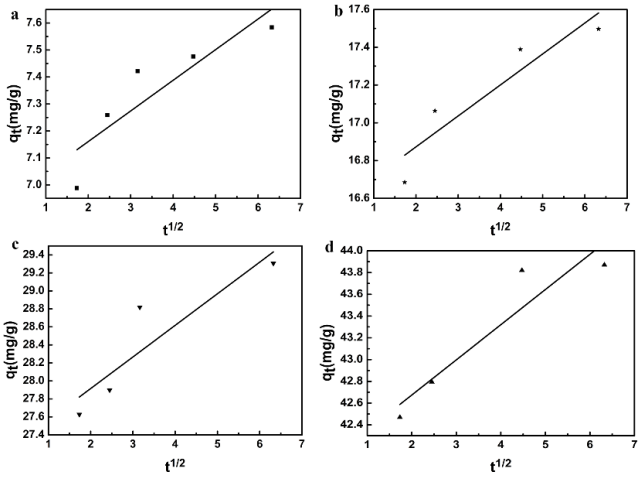

Fig. 7. Intra-particle diffusion model in the MB adsorption onto TRR at different MB concentrations: (a) 50, (b) 100, (c) 175 and (d) 250 mg/L.

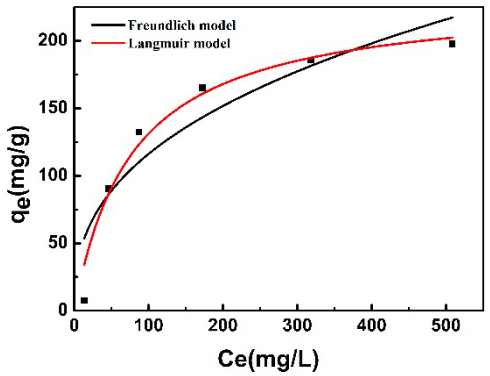

Fig. 8. Adsorption isotherms in the MB adsorption onto TRR.

Table 3
Parameters of intra-particle diffusion model

C_0 (mg/L)	k (mol/(g·min$^{1/2}$))	C (mg/g)	R^2
50	0.114	6.93	0.722
100	0.164	16.5	0.798
175	0.351	27.2	0.732
250	0.324	42.0	0.827

Table 4
Parameters of Langmuir and Freundlich equations for the adsorption of MB

Langmuir isotherm model				Freundlich isotherm model			
χ^2	R^2	q_m (mg/g)	b	χ^2	R^2	K_F	n
0.918	0.959	233.3	0.0129	9.812	0.902	19.8	2.60

R_L, a constant relies on Langmuir isotherm, is defined by the following relationship:

$$R_L = 1/(1 + bC_0) \quad (11)$$

where the C_0 is the initial concentration. The value of R_L indicates the type of the isotherm is irreversible ($R_L = 0$), favorable ($0 < R_L < 1$), linear ($R_L = 1$) or unfavorable ($R_L > 1$).

The values of R_L are from 0.049 to 0.608, which indicates the adsorption of MB onto TRR is favorable. The result is in agreement with the one obtained from Freundlich isotherm.

3.5.7. Adsorption thermodynamics

To evaluate the effect of temperature on adsorption process of MB onto TRR, the thermodynamic parameters such as Gibbs free energy (ΔG), enthalpy (ΔH) and entropy (ΔS) were calculated using the following two equations (Eqs. (12) and (13)).

The values of enthalpy (ΔH) and entropy (ΔS) were obtained according to Van't Hoff equation (Eq. (11)).

$$\ln(q_e/C_e) = -\Delta H/RT + \Delta S/R \quad (12)$$

The ΔG is given by the following equation (Eq. (13)):

$$\Delta G = \Delta H - T\Delta S \quad (13)$$

where the R and T are universal gas constant (8.314 J/(mol K)) and absolute temperature, respectively. ΔS and ΔH are calculated from the intercept and slope of the plot of $\ln(q_e/C_e)$ vs. $1/T$ (Fig. 9).

The thermodynamics values are given in Table 5. The negative values of ΔG for adsorption of MB onto TRR indicate the spontaneity of the adsorption process of the MB onto TRR. The ΔH is found to be negative, which indicates that the adsorption of MB onto TRR is exothermic. The data show that $|T\Delta S| < |\Delta H|$ at 298, 308 and 318 K, it indicates that the adsorption of MB onto TRR was an enthalpy-controlled process [36,37].

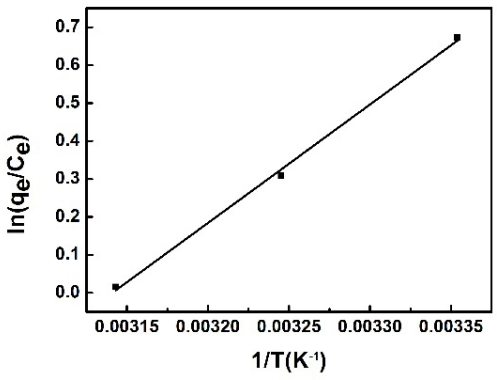

Fig. 9. Van't Hoff plots for MB adsorption on TRR.

3.5.8. Comparison of various adsorbents

The maximum monolayer adsorption capacity of MB onto TRR was compared with other adsorbents previously reported. As shown in Table 6, compared with the reported adsorbents, TRR shows fast adsorption and high maximum monolayer adsorption capacity. Though the maximum monolayer adsorption capacity is slightly smaller than lotus leaf, the adsorption rate is much faster than lotus leaf. It makes TRR promising for the practical applications as an effective adsorbent for removing MB.

3.6. Regeneration studies

The recycle and regeneration ability is important for the application of adsorbents. Thus, the recycle use of the adsorbents was studied. The TRR after adsorption of MB were desorbed by different eluants, such as 0.01 M HCl, 0.01 M NaOH and 0.01 M EDTA solutions. The results show that the percentage of desorption for TRR with 0.01 M HCl solution is the highest (83.7%). The high desorption efficiency at acidic condition may be that the H^+ ions compete for the adsorption sites with the cationic MB molecules [43]. Thus, the adsorption/desorption cycles for TRR were investigated by using 0.01 M HCl solution as eluant. The results of the adsorption–desorption cycles are shown in Fig. 10. It can be seen that the adsorption capacity decreased from 90.5 to 74.1 mg/g after four cycles. The adsorption capacity is still high. The results show a good prospect in the adsorption of MB on TRR in practical application.

3.7. Adsorption mechanism

Adsorption mechanism is very important to understand the adsorption process. The adsorption of MB on TRR is a complicated process as seen in Fig. 11.

According to the results of FT-IR, the hydrogen bonding interaction was formed between the nitrogen from MB and hydrogen from TRR. In most adsorption process, hydrogen bonds are present as non-electrostatic [44].

From the results of the effect of pH, the adsorption mechanism of the adsorption of MB onto TRR is inferred to electrostatic interaction.

Ion-exchange process was an important mechanism in MB adsorption on TRR, which can be supported by three results as follows:

(1) Low adsorption capacity in low pH.
(2) The adsorption capacity decrease with the increase of NaCl concentration, and the pH decrease in the same time.
(3) High desorption efficiency in acid situation.

Table 5
Thermodynamic parameters for MB adsorption on TRR

Temperature (K)	ΔH (kJ/mol)	ΔS (J/(mol·K))	ΔG (J/mol)	TΔS (kJ/mol)
298	–26.0	–81.5	–1,650	–24.35
308			–833	–25.17
318			–18.2	–25.98

Table 6
Comparison of adsorption capacities for MB with different adsorbents

Adsorbents	Adsorption time (min)	Adsorption capacities (mg/g)	Reference
Modified sepiolite	120	90.2	[38]
Algae Gelidium	–	171	[15]
Modified sawdust	–	111.5 (293 K)	[24]
Surfactant-modified wheat straw	60	126.6	[21]
Gulmohar	–	186.2	[25]
Lotus leaf	240	241.4	[26]
Peanut husk	–	72.13	[27]
Platanus orientalis, leaf powder	70	115	[19]
Tea waste	300	85.2	[16]
Sawdust	240	33.6	[20]
Garlic peel	130	82.6	[39]
Rejected tea	120	147	[40]
Rice husk	150	40.6	[17]
Osmanthus fragrans powder	40	165.0	[41]
Tobacco stems biomass	120	169.5	[42]
Tobacco rob residues	30	233.3	This work

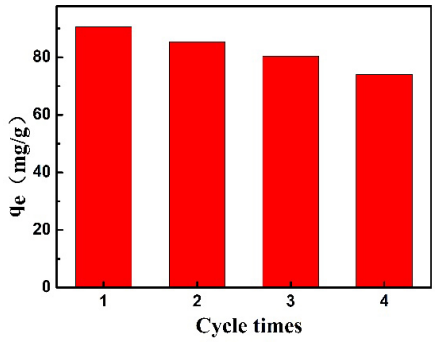

Fig. 10. Adsorption capacity of TRR for MB in four cycles.

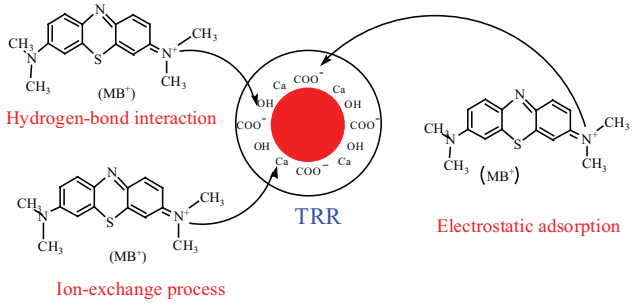

Fig. 11. Process of ion-exchange of MB on TRR.

Thus, the mechanism of MB adsorption onto TRR includes electrostatic interaction, ion exchange and hydrogen bond interaction.

4. Conclusions

The TRR was prepared by the extraction of tobacco rob using distilled water. Under the condition of the initial MB concentration of 250 mg/L, the adsorbent dosage of 5.0 g/L, the pH of 6.5 and the adsorption time of 10 min, the adsorption capacity of MB onto TRR can achieve 43.8 mg/g. The adsorption isotherms were found to be well represented by the Langmuir isotherm model. The maximum adsorption capacity for methylene blue onto TRR is 233.3 mg/g. The kinetics of MB adsorption onto TRR was best described by pseudo-second order model, which indicated that the MB adsorption process is a chemical process. FT-IR results suggest that the hydroxyl and carboxyl groups on TRR may facilitate MB adsorption. The mechanism of adsorption process of MB onto TRR includes electrostatic interaction, ion exchange and hydrogen bond interaction. Moreover, TRR shows facile recovery and recycling properties and has potential to be used as a good natural adsorbent for removal of MB.

Acknowledgments

This work was financially supported by the National Natural Science Foundation of China (No. 2176058) and the Natural Science Foundation of Hebei Province (No. B2017202226).

References

[1] R. Gong, M. Li, C. Yang, Y. Sun, J. Chen, Removal of cationic dyes from aqueous solution by adsorption on peanut hull, J. Hazard. Mater., 121 (2005) 247–250.
[2] Y. Bulut, H. Aydın, A kinetics and thermodynamics study of methylene blue adsorption on wheat shells, Desalination, 194 (2006) 259–267.
[3] S. Wang, Y. Boyjoo, A. Choueib, Z.H. Zhu, Removal of dyes from aqueous solution using fly ash and red mud, Water Res., 39 (2005) 129–138.
[4] S. Altenor, B. Carene, E. Emmanuel, J. Lambert, J. Ehrhardt, S. Gaspard, Adsorption studies of methylene blue and phenol onto vetiver roots activated carbon prepared by chemical activation, J. Hazard. Mater., 165 (2008) 1029–1039.
[5] Y. Kismir, A.Z. Aroguz, Adsorption characteristics of the hazardous dye Brilliant Green on Saklıkent mud, Chem. Eng. J., 172 (2011) 199–206.

[6] Y. Fu, T. Viraraghavan, Fungal decolorization of dye wastewaters: a review, Bioresour. Technol., 79 (2001) 251–262.
[7] J. Sheng, Y. Xie, Y. Zhou, Adsorption of methylene blue from aqueous solution on pyrophyllite, Appl. Clay Sci., 46 (2009) 422–424.
[8] S. Senthilkumaar, P.R. Varadarajan, K. Porkodi, C.V. Subbhuraam, Adsorption of methylene blue onto jute fiber carbon: kinetics and equilibrium studies, J. Colloid Interface Sci., 284 (2005) 78–82.
[9] V.K. Gupta, Suhas, Application of low-cost adsorbents for dye removal - a review, J. Environ. Manage., 90 (2009) 2313–2342.
[10] M. Kornaros, G. Lyberatos, Biological treatment of wastewaters from a dye manufacturing company using a trickling filter, J. Hazard. Mater., 136 (2006) 95–102.
[11] Y. Ku, L. Wang, C. Ma, Y. Chou, Photocatalytic oxidation of reactive red 22 in aqueous solution using $La_2Ti_2O_7$ photocatalyst, Water Air Soil Pollut., 215 (2011) 97–103.
[12] R. Gonzalez-Olmos, F. Holzer, F.D. Kopinke, A. Georgi, Indications of the reactive species in a heterogeneous Fenton-like reaction using Fe-containing zeolites, Appl. Catal., A, 398 (2011) 44–53.
[13] A.H. Jawad, M.A.M. Ishak, A.M. Farhan, K. Ismail, Response surface methodology approach for optimization of color removal and COD reduction of methylene blue using microwave-induced NaOH activated carbon from biomass waste, Desal. Wat. Treat., 62 (2017) 208–220.
[14] S. Yorgun, N. Karakehya, D. Yildiz, Adsorption of methylene blue onto activated carbon obtained from $ZnCl_2$ activation of paulownia wood: kinetic and equilibrium studies, Desal. Wat. Treat., 58 (2017) 274–284.
[15] V.J.P. Vilar, C.M.S. Botelho, R.A.R. Boaventura, Methylene blue adsorption by algal biomass based materials: biosorbents characterization and process behaviour, J. Hazard. Mater., 147 (2007) 120–132.
[16] M.T. Uddin, M.A. Islam, S. Mahmud, M. Rukanuzzaman, Adsorptive removal of methylene blue by tea waste, J. Hazard. Mater., 164 (2009) 53–60.
[17] V. Vadivelan, K.V. Kumar, Equilibrium, kinetics, mechanism, and process design for the sorption of methylene blue onto rice husk, J. Colloid Interface Sci., 286 (2005) 90–100.
[18] R. Han, Y. Wang, X. Zhao, Y. Wang, F. Xie, J. Cheng, M. Tang, Adsorption of methylene blue by phoenix tree leaf powder in a fixed-bed column: experiments and prediction of breakthrough, Desalination, 245 (2009) 284–297.
[19] M. Peydayesh, A. Rahbar-Kelishami, Adsorption of methylene blue onto *Platanus orientalis* leaf powder: kinetic, equilibrium and thermodynamic studies, J. Ind. Eng. Chem., 21 (2015) 1014–1019.
[20] H. Akrout, S. Jellali, L. Bousselmi, Enhancement of methylene blue removal by anodic oxidation using BDD electrode combined with adsorption onto sawdust, C.R. Chim, 18 (2015) 110–120.
[21] A.E. Pirbazari, S.F. Hashemian, A. Yousefi, Surfactant-modified wheat straw: preparation, characterization and its application for methylene blue adsorption from aqueous solution, J. Chem. Eng. Process Technol., 6 (2015) 595–606.
[22] H. Wang, M. Gao, Y. Guo, Y. Yang, R. Hu, A natural extract of tobacco rob as scale and corrosion inhibitor in artificial seawater, Desalination, 398 (2016) 198–207.
[23] Y. Guo, H. Wang, Z. Liu, Scale and corrosion inhibition performance of tobacco rob extract, Ciesc. J., 65 (2014) 298–304.
[24] H. Chen, J. Zhao, G.L. Dai, Silkworm exuviae—a new non-conventional and low-cost adsorbent for removal of methylene blue from aqueous solutions, J. Hazard. Mater., 186 (2011) 1320–1327.
[25] N.A.M. Razali, N. Azraaie, N.A.M.Z. Abidin, N.A. Ibrahim, F.A. Aziz1, S.A. Rahman, Preparation and XRD analysis of cellulose from merbau (*Intsia bijuga*), Adv. Mater. Res., 895 (2014) 151–154.
[26] G.W. Guo, S.J. Li, L. Wang, S.X. Ren, G.Z. Fang, Separation and characterization of lignin from bio-ethanol production residue, Bioresour. Technol., 135 (2013) 738–741.
[27] W. Zou, H. Bai, S. Gao, K. Li, Characterization of modified sawdust, kinetic and equilibrium study about methylene blue adsorption in batch mode, Korean J. Chem. Eng., 30 (2013) 111–122.
[28] V. Ponnusami, V. Gunasekar, S.N. Srivastava, Kinetics of methylene blue removal from aqueous solution using gulmohar (*Delonix regia*) plant leaf powder: multivariate regression analysis, J. Hazard. Mater., 169 (2009) 119–127.
[29] X. Han, W. Wang, X. Ma, Adsorption characteristics of methylene blue onto low cost biomass material lotus leaf, Chem. Eng. J., 171 (2011) 1–8.
[30] J. Song, W. Zou, Y. Bian, F. Su, R. Han, Adsorption characteristics of methylene blue by peanut husk in batch and column modes, Desalination, 265 (2011) 119–125.
[31] J. Fu, Z. Chen, X. Wu, M. Wang, X. Wang, J. Zhang, J. Zhang, Q. Xu, Hollow poly (cyclotriphosphazene-co-phloroglucinol) microspheres: an effective and selective adsorbent for the removal of cationic dyes from aqueous solution, Chem. Eng. J., 281 (2015) 42–52.
[32] S. Mak, D. Chen, Fast adsorption of methylene blue on polyacrylic acid-bound iron oxide magnetic nanoparticles, Dyes Pigm., 61 (2004) 93–98.
[33] P.S. Kumar, S. Ramalingam, C. Senthamarai, M. Niranjanaa, P. Vijayalakshmi, S. Sivanesan, Adsorption of dye from aqueous solution by cashew nut shell: studies on equilibrium isotherm, kinetics and thermodynamics of interactions, Desalination, 261 (2010) 52–60.
[34] H. Chen, J. Zhao, G.L. Dai, J.Y. Wu, H. Yan. Adsorption characteristics of Pb (II) from aqueous solution onto a natural biosorbent fallen *Cinnamomum camphora* leaves, Desalination, 262 (2010) 174–182.
[35] S. Wang, Y. Boyjoo, A. Choueib, A comparative study of dye removal using fly ash treated by different methods, Chemosphere, 60 (2005) 1401–1407.
[36] G.L. Dotto, J.M.N. Santos, I.L. Rodrigues, R. Rosa, F.A. Pavan, E.C. Lima, Adsorption of Methylene Blue by ultrasonic surface modified chitin, J. Colloid Interface Sci., 446 (2015) 133–140.
[37] A.M. Yousif, O.F. Zaid, I.A. Ibrahim, Fast and selective adsorption of As (V) on prepared modified cellulose containing Cu(II) moieties, Arab. J. Chem., 9 (2016) 607–615.
[38] Z. Cheng, R. Yang, X. Zhu, Adsorption behaviors of the methylene blue dye onto modified sepiolite from its aqueous solutions, Desal. Wat. Treat., 57 (2016) 25207–25215.
[39] B.H. Hameed, A.A. Ahmad, Batch adsorption of methylene blue from aqueous solution by garlic peel, an agricultural waste biomass, J. Hazard. Mater., 164 (2009) 870–875.
[40] N. Nasuha, B.H. Hameed, A.T.M. Din, Rejected tea as a potential low-cost adsorbent for the removal of methylene blue, J. Hazard. Mater., 175 (2010) 126–132.
[41] B. Chai, X. Cheng, Z. Ren, Y. Zhu, Biosorption of methylene blue from aqueous solution by natural *Osmanthus fragrans* powder, Desal. Wat. Treat., 57 (2016) 18868–18878.
[42] D.D. Reddy, R.K. Ghosh, J.P. Bindu, M. Mahadevaswamy, T.G.K. Murthy, Removal of methylene blue from aqueous system using tobacco stems biomass: kinetics, mechanism and single-stage adsorbent design, Environ. Prog. Sustain., 36 (2017) 1005–1012.
[43] Y. Li, Q. Du, T. Liu, J. Sun, Y. Wang, S. Wu, Z. Wang, Y. Xia, L. Xia, Methylene blue adsorption on graphene oxide/calcium alginate composites, Carbohydr. Polym., 95 (2013) 501–507.
[44] S. Fan, Y. Wang, Z. Wang, J. Tang, J. Tang, X. Li, Removal of methylene blue from aqueous solution by sewage sludge-derived biochar: adsorption kinetics, equilibrium, thermodynamics and mechanism, J. Environ. Chem. Eng., 5 (2017) 601–611.